CHARACTERIZATION OF LAYERED ANISOTROPIC MEDIA BY ULTRASONIC WAVES: MODELING AND EXPERIMENT

S. I. Rokhlin, L. Wang
The Ohio State University, Nondestructive Evaluation Program, Edison Joining Technology Center,
1248 Arthur E. Adams Drive, Columbus, Ohio 4322, USA
rokhlin.2@osu.edu

Abstract

Recent advances in ultrasonic wave propagation in layered arbitrarily anisotropic media are reviewed. New exact and asymptotic approaches based on an efficient and stable recursive compliance/stiffness matrix method are presented. In the asymptotic method, the total stiffness matrix for the system of multilayers is calculated with arbitrary precision by subdividing them into thin sublayers and combining recursively the thin layer stiffness matrices which are obtained based on a simple second-order thin layer approximation. A semi-space substrate is substituted for by a finite thickness layer loaded by a perfectly matched attenuating layer. Both methods are applied to direct and inverse problems of ultrasonic characterization of multidirectional composites using the double-through-transmission method and time-resolved line focus acoustic microscopy. The double-through-transmission measurements and simulations show that the transmission amplitude is highly dependent on ply orientation and angle of incidence. As another example surface acoustic wave propagation in a multilayered piezoelectric medium is considered. To do this the effective permittivity and general Green's functions for a layered piezoelectric system on a substrate are formulated in terms of stiffness and compliance matrices.

Introduction

The topic of elastic wave propagation in layered media has enjoyed significant attention for many decades due to the wealth of its applications to seismology, acoustics and nondestructive evaluation (NDE) [1-29]. In most ultrasonic applications the transfer matrix method formulated by the Stroh representation [5, 9] or the Christoffel equation [10, 11] has been utilized. However the method becomes inherently unstable due to the coexistence of exponentially decaying and growing matrix elements, a problem that has been known as 'exponential dichotomy" in the numerical solution of linear matrix differential equations [12]. To overcome the computational instabilities, a reformulation based on the higher-order minors of the transfer matrix (delta matrix method) has been developed for isotropic layered systems [4, 13] and has also been proposed for monoclinic layers [13]. But for the general anisotropic medium this method is impractical due to its inefficiency and complexity. Various other computationally robust methods have been developed such as the global matrix method [7, 8], the reflectivity method [14-16] (also called the invariant embedding method) and its variations based on surface impedance matrices [17]. Recently an alternative stable computation method for general anisotropic layered media based on the stiffness matrix method [18-21] has been developed. In this method, the generalized surface compliance/stiffness matrix for a layered substrate and the total compliance/stiffness matrix for a multilayered system are calculated recursively from the layer stiffness matrices. The method retains the efficiency and simplicity of the transfer matrix method but is stable. More recently the recursive stiffness matrix method has been further simplified using an explicit second order asymptotic representation [22, 23].

One of the important applications for ultrasonic waves in layered media is quantitative nondestructive evaluation of multidirectional composites. Multidirectional composites are highly anisotropic multilayered structures, which significantly complicates ultrasonic wave propagation [24-27]. Selection of ultrasonic inspection parameters is very difficult for these structures without comprehensive modeling for optimization of the experimental conditions and data interpretation. In this paper, recent advances in ultrasonic wave propagation in layered arbitrarily anisotropic media are reviewed and their applications to surface acoustic wave analysis and composite material characterization are discussed.

Ultrasonic models for layered anisotropic media

Exact transfer and stiffness matrices for an anisotropic layer

Let us consider generally anisotropic piezoelectric media as shown in Fig.1. We define the general displacement $\mathbf{U}$ (=[$\mathbf{u}$, ϕ]^T) and general stress $\mathbf{T}$ =[$\boldsymbol{\sigma}$, D_3]^T vectors and the state vector $\boldsymbol{\xi} = \begin{bmatrix} \mathbf{U} \\ \mathbf{T} \end{bmatrix}$, where $\mathbf{u}$ and $\boldsymbol{\sigma}$ are the particle displacement and normal stress vectors respectively, and ϕ and D_3 are the electrical potential and normal electric displacement respectively. The general solution for the state vector

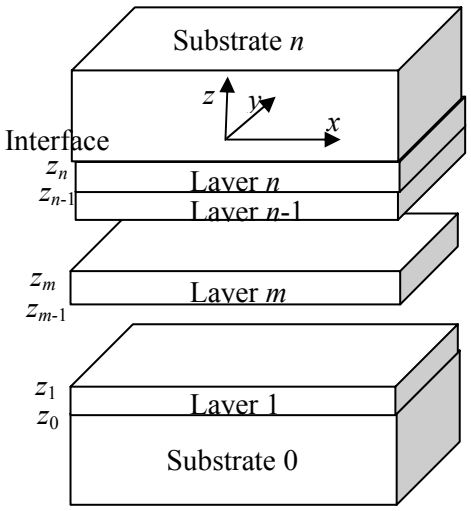

Figure 1: A layered general anisotropic structure and coordinate system. The z-axis is normal to the layer surface. The top and bottom surfaces can be free or bounded by the substrates.

can be represented in the form $\boldsymbol{\xi}(z)e^{i(\omega t-k_x x)}$, where ω is angular frequency, k_x is the wave number along the x-axis. The governing equation for the state vector is [5, 21]

$$\frac{d\boldsymbol{\xi}}{dz} = i\mathbf{A}\boldsymbol{\xi}, \tag{1}$$

where $\mathbf{A}$ is the fundamental acoustic tensor; it is explicitly given in Appendix A. For a single homogeneous layer, e.g., the mth layer, the differential equation (1) has the well-known exponential transfer matrix solution $\mathbf{B}$, which relates the state vector at the layer top (z_m) to that at the layer bottom (z_{m-1}) surface

$$\boldsymbol{\xi}(z_m) = \mathbf{B}\boldsymbol{\xi}(z_{m-1}),\ \mathbf{B} = e^{i\mathbf{A}H_m}, \tag{2}$$

where H_m=z_m-z_{m-1} is the thickness of the m^{th} layer. To compute $\mathbf{B}$ requires finding the eigenvalues k_z and eigenvector matrix $\mathbf{W}$ of the fundamental matrix $\mathbf{A}$. For general anisotropic material with piezoelectricity there are eight eigenvalues and eigenvectors representing eight plane harmonic waves. Four waves propagate (or exponentially decay) in the $+z$ direction and we denote the corresponding eigenvalues as $\boldsymbol{\beta}_z^+ = \mathbf{I}\ \text{diag}(k_z^{+1}, k_z^{+2}, k_z^{+3}, k_z^{+4})$ ($\mathbf{I}$(4×4) is a unit matrix) and the corresponding eigenvector matrix as $\mathbf{W}^+ = [\mathbf{P}^+\ \mathbf{D}^+]^{\mathrm{T}}$, where $\mathbf{P}^+$ corresponds to the general displacement portion and $\mathbf{D}^+$ to the general stress portion in the eigenvector matrix $\mathbf{W}^+$. The other four waves propagate (or exponentially decay) in the $-z$ direction and we denote their eigenvalues as $\boldsymbol{\beta}_z^- = \mathbf{I}\ \text{diag}(k_z^{-1}, k_z^{-2}, k_z^{-3}, k_z^{-4})$ and the eigenvector matrix as $\mathbf{W}^- = \begin{bmatrix}\mathbf{P}^- & \mathbf{D}^-\end{bmatrix}^{\mathrm{T}}$. The canonical (diagonalized) form of the matrix $\mathbf{A}$ is represented as

$$\mathbf{A} = \mathbf{W}\boldsymbol{\beta}_z\,\mathbf{W}^{-1} = \begin{bmatrix}\mathbf{P}^- & \mathbf{P}^+\\ \mathbf{D}^- & \mathbf{D}^+\end{bmatrix}\begin{bmatrix}\boldsymbol{\beta}_z^- & \mathbf{0}\\ \mathbf{0} & \boldsymbol{\beta}_z^+\end{bmatrix}\begin{bmatrix}\mathbf{P}^- & \mathbf{P}^+\\ \mathbf{D}^- & \mathbf{D}^+\end{bmatrix}^{-1}, \tag{3}$$

where $\boldsymbol{\beta}_z = \begin{bmatrix}\boldsymbol{\beta}_z^- & \mathbf{0}\\ \mathbf{0} & \boldsymbol{\beta}_z^+\end{bmatrix}$. From Eqs. (2) and (3) it follows that $\mathbf{B} = \mathbf{W}e^{i\boldsymbol{\beta}_z H_m}\mathbf{W}^{-1}$ and we can obtain

$$\begin{bmatrix}\mathbf{U}(z_m)\\ \mathbf{T}(z_m)\end{bmatrix} = \mathbf{B}\begin{bmatrix}\mathbf{U}(z_{m-1})\\ \mathbf{T}(z_{m-1})\end{bmatrix};$$
$$\mathbf{B} = \begin{bmatrix}\mathbf{P}^- & \mathbf{P}^+\mathbf{H}^+\\ \mathbf{D}^- & \mathbf{D}^+\mathbf{H}^+\end{bmatrix}\begin{bmatrix}\mathbf{P}^-\mathbf{H}^- & \mathbf{P}^+\\ \mathbf{D}^-\mathbf{H}^- & \mathbf{D}^+\end{bmatrix}^{-1}, \tag{4}$$

where matrix $\mathbf{H}^{\pm}(4\times 4) = \mathbf{I}\ \text{diag}[e^{\pm ik_z^{\pm 1}H_m},\ e^{\pm ik_z^{\pm 2}H_m},\ e^{\pm ik_z^{\pm 3}H_m}, e^{\pm ik_z^{\pm 4}H_m}]$. In Eq. (4), we combine the diagonal matrix $\mathbf{H}^+$ with $\mathbf{W}$ and $(\mathbf{H}^-)^{-1}$ with $\mathbf{W}^{-1}$.

To improve the computational stability, we reformulate the transfer matrix in the form of a stiffness matrix [20], which relates displacements on both sides of the layer to the stress

$$\begin{bmatrix}\mathbf{T}(z_m)\\ \mathbf{T}(z_{m-1})\end{bmatrix} = \mathbf{K}\begin{bmatrix}\mathbf{U}(z_m)\\ \mathbf{U}(z_{m-1})\end{bmatrix};$$
$$\mathbf{K} = \begin{bmatrix}\mathbf{K}_{11} & \mathbf{K}_{12}\\ \mathbf{K}_{21} & \mathbf{K}_{22}\end{bmatrix} = \begin{bmatrix}\mathbf{D}^- & \mathbf{D}^+\mathbf{H}^+\\ \mathbf{D}^-\mathbf{H}^- & \mathbf{D}^+\end{bmatrix}\begin{bmatrix}\mathbf{P}^- & \mathbf{P}^+\mathbf{H}^+\\ \mathbf{P}^-\mathbf{H}^- & \mathbf{P}^+\end{bmatrix}^{-1}. \tag{5}$$

We also define an inverse compliance matrix $\mathbf{S}$:

$$\mathbf{S} = \mathbf{K}^{-1} = \begin{bmatrix}\mathbf{S}_{11} & \mathbf{S}_{12}\\ \mathbf{S}_{21} & \mathbf{S}_{22}\end{bmatrix} = \begin{bmatrix}\mathbf{P}^- & \mathbf{P}^+\mathbf{H}^+\\ \mathbf{P}^-\mathbf{H}^- & \mathbf{P}^+\end{bmatrix}\begin{bmatrix}\mathbf{D}^- & \mathbf{D}^+\mathbf{H}^+\\ \mathbf{D}^-\mathbf{H}^- & \mathbf{D}^+\end{bmatrix}^{-1}. \tag{6}$$

The symmetry properties of the compliance/stiffness matrix are given in ref. 21.

For a semi-infinite medium, one can define a surface stiffness matrix $\mathbf{K}_S$ which relates the general displacement to the general stress at the surface

$$\mathbf{T}_{\pm} = \mathbf{K}_S^{\pm}\mathbf{U}_{\pm},\ \mathbf{K}_S^{\pm} = \mathbf{D}^{\pm}(\mathbf{P}^{\pm})^{-1}, \tag{7}$$

where $\mathbf{K}_S^+$ is the surface stiffness matrix for a bottom half space and $\mathbf{K}_S^-$ is the surface stiffness matrix for a top half space. For a layer with attenuation or for nonhomogeneous wave propagation, as the thickness of the layer approaches infinity, both matrices $\mathbf{H}^{\pm}$

become zero; then from Eqs.(5, 7) one can see that the submatrices $\mathbf{K}_{11}$ and $\mathbf{K}_{22}$ approach the surface stiffness matrices $\mathbf{K}_S^-$ and $\mathbf{K}_S^+$ respectively.

Asymptotic transfer and stiffness matrices for an anisotropic layer

In this section we briefly review a much simpler solution of the problem [22]. First let us consider the asymptotic solution for a thin layer whose thickness h is much less than the ultrasonic wavelength λ ($h/\lambda << 1$). A second-order asymptotic solution for the transfer matrix has been proposed by Rokhlin and Huang [28], which can be written as

$$\mathbf{B}_{\mathrm{II}} = (\mathbf{I} - i\frac{h}{2}\mathbf{A})^{-1}(\mathbf{I} + i\frac{h}{2}\mathbf{A}). \qquad (8)$$

The advantage of the asymptotic transfer matrix representation Eq. (8) is that it has the same symmetry properties as the exact transfer matrix and the wave solution obtained with the transfer matrix (8) satisfies energy balance for wave interaction with a thin layer. As was shown in ref. 28, this is due inherently to the representation of the transfer matrix $\mathbf{B}_{\mathrm{II}}$ in the form (8).

The asymptotic solution (8) is valid only for a thin layer. For a thick layer with thickness H_m, one can subdivide it into N thin layers and the total asymptotic transfer matrix $\mathbf{B}_a(H_m)$ for a thick layer is obtained as the product of all thin layer transfer matrices. For computational efficiency, one should select N as a power of 2 (N=2^n), then for a homogeneous layer H_m the number of matrix multiplications is n if $\mathbf{B}_a$ is calculated recursively as

$$\mathbf{B}_a^{(J)} = \mathbf{B}_a^{(J-1)}\mathbf{B}_a^{(J-1)}, \qquad (9)$$

where (J) =(1),….(n) is a running index; $\mathbf{B}_a^{(0)} = \mathbf{B}_{\mathrm{II}}(h)$; $\mathbf{B}_a^{(J)} = \mathbf{B}_a(2^j h)$ is the total asymptotic transfer matrix at step J; $\mathbf{B}_a^{(J-1)} = \mathbf{B}_a(2^{j-1}h)$ and H_m =2$^n h$. The solution obtained thus converges to the exact solution [22].

To assure computational stability of the solution we have to employ the asymptotic stiffness matrix. The asymptotic stiffness matrix for a thin layer is obtained using the relation between the transfer **B** and the stiffness **K** matrices [20]; the corresponding second-order stiffness matrix $\mathbf{K}_{\mathrm{II}}$ is :

$$\mathbf{K}_{\mathrm{II}} = \begin{bmatrix} -\frac{\mathbf{\Gamma}_{33}}{h} + (\mathbf{\Gamma}_{31} - \mathbf{\Gamma}_{13})\frac{ik_x}{2} - \frac{\mathbf{\Gamma}_{11}hk_x^2}{4} + \frac{\rho h\omega^2}{4}\mathbf{I}' & \frac{\mathbf{\Gamma}_{33}}{h} + (\mathbf{\Gamma}_{31} + \mathbf{\Gamma}_{13})\frac{ik_x}{2} - \frac{\mathbf{\Gamma}_{11}hk_x^2}{4} + \frac{\rho h\omega^2}{4}\mathbf{I}' \\ -\frac{\mathbf{\Gamma}_{33}}{h} + (\mathbf{\Gamma}_{31} + \mathbf{\Gamma}_{13})\frac{ik_x}{2} + \frac{\mathbf{\Gamma}_{11}hk_x^2}{4} - \frac{\rho h\omega^2}{4}\mathbf{I}' & \frac{\mathbf{\Gamma}_{33}}{h} + (\mathbf{\Gamma}_{31} - \mathbf{\Gamma}_{13})\frac{ik_x}{2} + \frac{\mathbf{\Gamma}_{11}hk_x^2}{4} - \frac{\rho h\omega^2}{4}\mathbf{I}' \end{bmatrix}, \qquad (10)$$

where the submatrices $\mathbf{\Gamma}_{ij}$ are combinations of the elastic constants c_{ijk} (Appendix A). The asymptotic stiffness matrix elements are simple explicit functions of the elastic and piezoelectric properties. To find the stiffness matrix of a thick layer, as discussed above the thick layer H_m is subdivided into N=2^n thin layers h= H_m /N and the total stiffness matrix of the thick layer is obtained from the thin layer stiffness matrix using a recursive algorithm [22]:

$$\mathbf{K}_a^J = \begin{bmatrix} \mathbf{K}_{11}^{J-1} + \mathbf{K}_{12}^{J-1}(\mathbf{K}_{11}^{J-1} - \mathbf{K}_{22}^{J-1})^{-1}\mathbf{K}_{21}^{J-1} & -\mathbf{K}_{12}^{J-1}(\mathbf{K}_{11}^{J-1} - \mathbf{K}_{22}^{J-1})^{-1}\mathbf{K}_{12}^{J-1} \\ \mathbf{K}_{21}^{J-1}(\mathbf{K}_{11}^{J-1} - \mathbf{K}_{22}^{J-1})^{-1}\mathbf{K}_{21}^{J-1} & \mathbf{K}_{22}^{J-1} - \mathbf{K}_{21}^{J-1}(\mathbf{K}_{11}^{J-1} - \mathbf{K}_{22}^{J-1})^{-1}\mathbf{K}_{12}^{J-1} \end{bmatrix} \qquad (11)$$

where J=1,…n; $\mathbf{K}_a^J$ is the total asymptotic stiffness matrix after J recursive operations and $\mathbf{K}_{ij}^0$ are the submatrices of the thin layer asymptotic stiffness matrix $\mathbf{K}_{\mathrm{II}}$. As in the case of the asymptotic transfer matrix, to obtain the total stiffness matrix for N=2^n subdivisions only n recursive operations are required.

To illustrate the convergence of the asymptotic transfer and stiffness matrices, we define the relative error $E(\mathbf{B})/E(\mathbf{K})$ as the average relative error between the asymptotic and exact transfer/stiffness matrix elements ($\mathbf{B}[i,j]/\mathbf{K}[i,j]$)

$$E(\mathbf{B}) = \frac{1}{64}\sum_{i=1}^{8}\sum_{j=1}^{8}\left|(\mathbf{B}_a[i,j] - \mathbf{B}[i,j])/\mathbf{B}[i,j]\right|, \qquad (12a)$$

$$E(\mathbf{K}) = \frac{1}{64}\sum_{i=1}^{8}\sum_{j=1}^{8}\left|(\mathbf{K}_a[i,j] - \mathbf{K}[i,j])/\mathbf{K}[i,j]\right|. \qquad (12b)$$

The "exact" transfer and stiffness matrices are obtained by calculating the eigenvectors and eigenvalues of matrix **A** using Eqs (4 and 5). To investigate the convergence rate and the accumulation of round-off error with increase of number of subdivisions N=2^n, we plot in Fig. 2 the average relative error $E(\mathbf{B})$ and $E(\mathbf{K})$ versus number of recursive operations n at 1 GHz for a ZnO layer with thickness H=1 μm. Both $E(\mathbf{B})$ and $E(\mathbf{K})$ are averaged for a phase velocity (ω/k_x) in the range between 1 and 20 mm/μs. The calculation is performed with double precision. One can see that initially the relative error decreases exponentially as $(H_m/2^n)^2$ with increase of number of recursive operations n. This is because with

increase of n the thickness of the subdivision layers $h=H_m/2^n$ exponentially decreases for a given H_m, which leads to exponential decrease of the truncation error. As the number of recursive operations reaches a critical point, the error starts to increase due to the accumulation of round-off error resulting from multiplication of a large number of asymptotic transfer matrices.

The total relative error is the sum of the truncation and round-off errors. The total relative errors $E(\mathbf{B})$, $E(\mathbf{K})$ for both matrices are obtained as

$$E(\mathbf{B}) = \alpha_0 4^{-n} + e_0 2^n, E(\mathbf{K}) = \alpha_0 4^{-n} + e_0 4^n, \quad (13)$$

where $\alpha_0 = \frac{1}{3}(\frac{\pi f H_m}{V_{qs}})^2$ and $e_0 = 10^{-16}$. The minimum of the average relative error corresponds to the optimum number n_{opt} of recursive operations. It is obtained from Eq. (13):

$$n_{\text{opt}}(\mathbf{B}) = \tfrac{1}{3}(1 + \log_2 \tfrac{\alpha_0}{e_0}), \; n_{\text{opt}}(\mathbf{K}) = \tfrac{1}{4}\log_2 \tfrac{\alpha_0}{e_0}. \quad (14)$$

The growth rate of the round-off error is proportional to 2^n for the transfer matrix. The growth rate of the stiffness matrix round-off error is proportional to $(2^n)^2$ and is twice that of the transfer matrix. To take advantage of both methods (the smaller round-off error for the transfer matrix and the stability of the stiffness matrix for larger fH_m) we propose a hybrid (**B**/**K**) method. In this method, we start the recursive

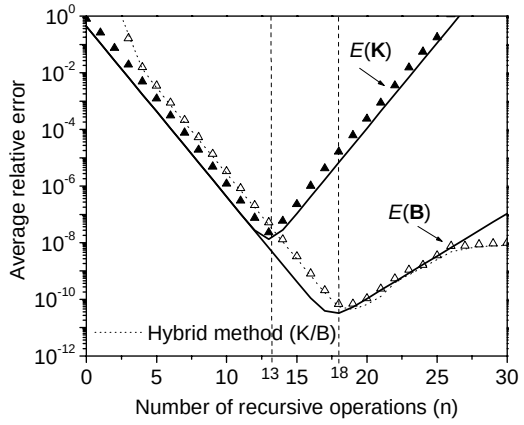

Figure 2: Simulated (solid lines calculated using Eq. 13) and actual relative error for stiffness (**K**) and transfer (**B**) matrices for a ZnO layer at fH=1 GHz*μm. The number of layer subdivisions N is 2^n. The relative error averaged in the phase velocity (ω/k_x) range between 1.0 and 20.0mm/μs. The dotted line represents the result calculated by the hybrid method with δ=10. The predicted optimum recursive operations (n_{opt}) using Eq. 14 are indicated by the dashed lines.

procedure using the asymptotic transfer matrix (Eqs. 7 and 8). At each recursive step we calculate the average of the matrix $\mathbf{B}_a$ diagonal elements as a control parameter

$$\delta = \frac{1}{8}\sum_{i=1}^{8} \left|\mathbf{B}_a(i,i)\right|. \quad (15)$$

If nonhomogeneous waves exist, the nondimensional parameter δ starts to increase exponentially with the number of recursive operations j (the layer thickness $H_j=2^j h$). When δ exceeds a pre-selected threshold δ_c, we convert the transfer matrix obtained to the stiffness matrix, and then continue the recursive operation algorithm using the stiffness matrix recursive algorithm (Eq. 11). The optimum value of the threshold δ_c is around 10. The hybrid method has the same round-off error as the transfer matrix and is unconditionally stable.

Asymptotic surface stiffness matrix for a semispace

The exact wave propagation solution for a semispace is obtained using Eq. (7). To use the asymptotic method, one may replace the semispace by a thick layer with appropriate wave attenuations. For a sufficiently thick layer, the propagating waves inside the layer attenuate and the layer stiffness matrix converges to the surface stiffness matrix; however this method could require an excessive number of recursive operations. For this reason it is advantageous to accelerate the decay of wave amplitudes in the finite thickness layer. To do so we replace the substrate by a layer with artificial attenuation (perfectly-matched layer (PML)), which however does not change the surface stiffness matrix. The second-order asymptotic transfer $\mathbf{B}_{\text{II}}$ and stiffness $\mathbf{K}_{\text{II}}$ matrices solution for such a medium are obtained by the replacement of h by $h^*=h\beta$. β is a complex parameter (1.0, β_i) with $0<\beta_i<0.5$. Because β is complex all acoustic wave energy transmitted into the PML is attenuated.

Recursive algorithm to obtain the total compliance/ stiffness matrix

After the stiffness matrix $\mathbf{K}^m$ for each layer in the multilayered structure has been obtained using either the exact formulation or asymptotic solutions, the global stiffness matrix for the multilayered structure is calculated using a recursive algorithm

$$\mathbf{K}^M = \begin{bmatrix} \mathbf{K}_{11}^m + \mathbf{K}_{12}^m(\mathbf{K}_{11}^{M-1} - \mathbf{K}_{22}^m)^{-1}\mathbf{K}_{21}^m & -\mathbf{K}_{12}^m(\mathbf{K}_{11}^{M-1} - \mathbf{K}_{22}^m)^{-1}\mathbf{K}_{12}^{M-1} \\ \mathbf{K}_{21}^{M-1}(\mathbf{K}_{11}^{M-1} - \mathbf{K}_{22}^m)^{-1}\mathbf{K}_{21}^m & \mathbf{K}_{22}^{M-1} - \mathbf{K}_{21}^{M-1}(\mathbf{K}_{11}^{M-1} - \mathbf{K}_{22}^m)^{-1}\mathbf{K}_{12}^{M-1} \end{bmatrix} \quad (16)$$

where $\mathbf{K}^M$ are the asymptotic or exact total stiffness matrices for the bottom m layers, $\mathbf{K}_{ij}^{M-1}$ are the submatrices of the total stiffness matrix for the bottom m-1 layers, $\mathbf{K}_{ij}^{m}$ are the submatrices of the mth layer stiffness matrix. Alternatively, the top surface stiffness $\mathbf{K}_S$ for the total system may be obtained directly by calculating recursively only the $\mathbf{K}_{11}^M = \mathbf{K}_S^M$ submatrix.

Applications to ultrasonic characterization of multilayered anisotropic media

Angle beam through transmission: experiment and simulation

Ultrasonic evaluation of composites is usually performed by the immersion method in reflection or through-transmission modes. At oblique incidence of ultrasonic waves on a multidirectional composite, the reflection/transmission phenomena become very complicated [27] due to the appearance of nontransmittance zones. The plane wave reflection and transmission coefficients are related to the total compliance matrix of the composite laminate as [20]

$$T = \frac{2\Lambda S_{21}^{33}}{(S_{11}^{33}+\Lambda)(S_{22}^{33}-\Lambda)-S_{21}^{33}S_{12}^{33}}, \qquad (17)$$

$$R = \frac{(S_{11}^{33}-\Lambda)(S_{22}^{33}-\Lambda)-S_{21}^{33}S_{12}^{33}}{(S_{11}^{33}+\Lambda)(S_{22}^{33}-\Lambda)-S_{21}^{33}S_{12}^{33}}, \qquad (18)$$

where the S_{ij}^{33} are the (3, 3) elements in the submatrices $\mathbf{S}_{ij}(3\times3)$ of the total (6×6) compliance matrix $\mathbf{S}$ for the composite structure and $\Lambda = \cos\theta/(i\omega\rho_f V_f)$, ρ_f is the fluid density, and V_f is the acoustic velocity in the fluid, θ is the incident angle.

Here we will show an example of ultrasonic wave transmission through a $[0/45/90/-45]_{2s}$ composite in the double-through-transmission mode shown schematically in Figure 3. The ultrasonic signal is transmitted through the multiply composite sample immersed in the fluid, then reflected from the plane reflector and returned to the transducer. The sample is rotated in two planes, thus angles of incidence and plane of incidence can be continuously changed. We consider the back reflector as a mirror with Figure 3b showing the wave travel path used in the model. Accounting for the phase delay in fluid as shown in Fig. 3b, one can obtain the time-domain voltage output [27]:

$$V_{out}(t) = \int_{-\infty}^{+\infty} F(\omega)e^{i\omega t}d\omega \int_{-\infty}^{+\infty} \Phi_t(k_x')T_t(k_x)T_b(k_x'')e^{i(-2k_z'L+k_zd+k_z''d)}dk_x', \qquad (19)$$

where L is the distance between the surfaces of the transducer and back reflector, d is the thickness of the sample. $k_z = \sqrt{(\omega/V_f)^2 - k_x^2}$. k_x', k_z' and k_x'', k_z'' are the wave numbers in the coordinate systems rotated from the axis z (Figure 3b) by θ_i (primed) and $2\theta_i$ (double primed) respectively (z' is the normal to the transducer face). $F(\omega)$ is the frequency response of the transmitter/receiver; $\Phi_t(k_x')$ is the angular response of the transducer.

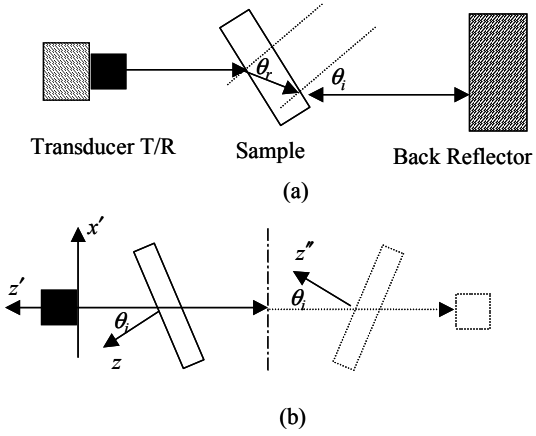

Figure 3: (a) Schematic diagram of the self-reference bulk wave method. (b) Equivalent representation of the measurement used for modeling. The dashed lines indicate the mirror reflection of the back propagation path. Mirror plane is indicated by the broken vertical line.

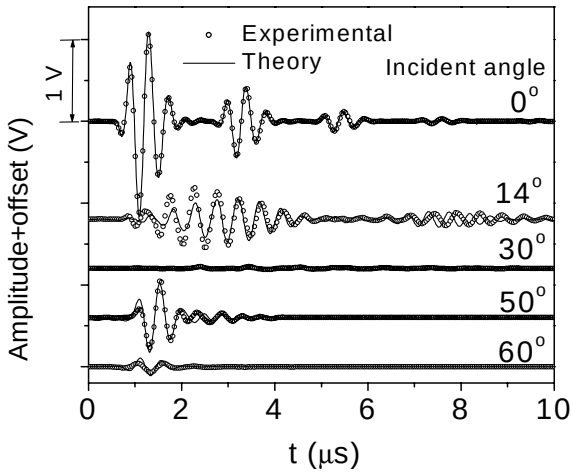

Figure 4: Experimental (open circles) and theoretical (solid lines) time domain signal of different incident angles. The rotation angle α is 25° and center frequency of the signals is 2.25 MHz.

They are experimentally determined by inverting the measured reflection signal from a homogeneous semispace such as a block of aluminum. $T_t(k_x)$ and $T_b(k_x'')$ are the plane wave transmission coefficients through the layer for the wave incident from fluid on the layer top or bottom respectively.

Figure 4 compares experimental (dots) and computed (solid lines) time domain signals for several incident angles. The incident wave signal has center frequency 2.25MHz. At normal incidence (0^o), the multiple reflections in the sample are clearly identified. At incident angles close to normal incidence ($<7^o$), the multilayered composite is similar to an isotropic plate. At 14^o incident angle, the transmitted signal reaches the first maximum and clearly shows dispersion and strong distortion. Above 14^o the amplitude drops, reaching the noise level at 30^o. The transmitted signal amplitude reaches an additional maximum at 50^o whereas spectrum analysis shows the center transmitted frequency at about 2 MHz. A large transmission peak appears in the incident angle range between 45^o to 55^o, where the energy is transmitted in the composite by the slow transverse wave. Above 60^o incident angle, the transmission amplitude drops again and approaches to zero.

Time-resolved line focus acoustic microscopy: experiment and simulation

As another example we will compare modeling and experimental results for the line focus acoustic microscopy. A cylindrically shaped line focus transducer is utilized with the coupling fluid between

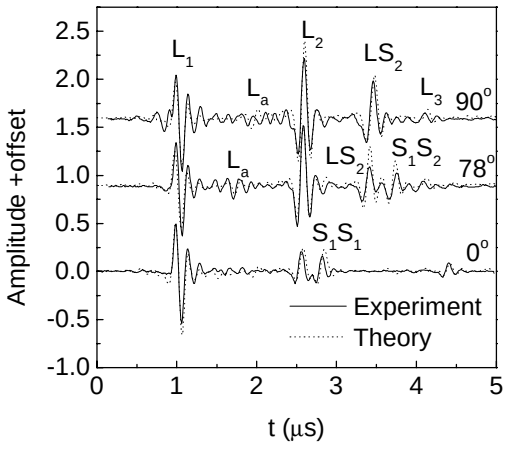

Figure 5: Line focus microscopy signature at different rotation angles for the unidirectional composite plate with thickness 2.4mm.The cylindrical transducer with PVDF film has center frequency 6MHz and focus length 24.5mm. Solid lines are experiment; doted lines are simulations.

transducer and specimen. For line focus time-resolved acoustic microscopy, the response can be represented as [26]

$$V_{out}(z,t) = \int_{-\infty}^{+\infty} F(\omega) e^{i\omega t} d\omega \int_0^{\theta_M} P(\theta) R(\theta,\omega) e^{2i\frac{\omega}{V_f} d_0 \cos\theta} d\theta, \quad (20)$$

where $F(\omega)$ is the frequency and $P(\theta)$ is the pupil function of the transducer in the pulse echo mode, θ_M is the semi-aperture angle of the acoustic lens and d_0 is the defocus distance. $R(\theta,\omega)$ is the reflection coefficient from the sample,

Our experiments were performed with the line focus transducer, developed at NIST [29], which has center frequency 6MHz, focus length 24.5mm and half aperture angle 32^o. Figure 5 shows the acoustic microscopy response for a unidirectional composite plate for different lens orientation with relation to the fiber direction. In these figures solid lines are experiment and dotted lines are theory. For a unidirectional composite as shown in Figure 5, the signals in the response can be put in three categories [26]: 1) normal specular reflections which correspond to normal incident rays (L_1 and L_2); 2) lateral waves which correspond to rays incident at critical angles (L_a); 3) bulk wave reflections which correspond to rays mode-converted and reflected from the bottom surface (LS_2, S_1S_1, S_1S_2; L denotes longitudinal and S_1, S_2 denote fast and slow quasi-transverse waves). The time delays of the normal specular reflections (L_1 and L_2) are used to determine the elastic constant C_{33} ($=C_{22}$). These signals are not shifted in the time domain with rotation angle. The time delays and amplitudes of these lateral wave and bulk wave reflections are significantly dependent on the rotation angle. Because the half aperture angle of our transducer is 32^o, only the longitudinal lateral wave (L_a) has been observed. The leaky surface wave does not exist [26] in these materials since its speed increases above the transverse wave speed due to the fluid loading effect. The lamina elastic constants have been obtained by a least-squares minimization algorithm to match the computed and experimental signatures [26].

Surface acoustic wave analysis

As an additional example let us consider a method to compute ultrasonic wave propagation in a layered piezoelectric medium. For this it is advantageous to use the generalized Green's function **G** and effective permittivity ε_{eff}. They are determined from the total surface stiffness matrix for the layered substrate or the total stiffness matrix for a layered plate. Here we use the layered semispace with surface transducers as an

example. For simplicity, we use the total surface compliance matrix $\mathbf{S}_S = \mathbf{K}_S^{-1}$ and decompose it into mechanical $\mathbf{S}_S^f$ (3×3), electric S_S^e (1×1) and coupling $\mathbf{S}_S^{fe}$ (3×1), $\mathbf{S}_S^{ef}$ (1×3) submatrices: $\mathbf{S}_S = \begin{bmatrix} \mathbf{S}_S^f & \mathbf{S}_S^{fe} \\ \mathbf{S}_S^{ef} & S_S^e \end{bmatrix}$. Taking into account the electric field in the vacuum above the top semi-space, where the electric potential satisfies the Laplace equation, the generalized surface Green's function can be written as

$$\mathbf{G} = \begin{bmatrix} \mathbf{S}_S^f + \alpha |k_x| \varepsilon_0 \mathbf{S}_S^{fe} \mathbf{S}_S^{ef} & -(1+\alpha |k_x| \varepsilon_0) \mathbf{S}_S^{fe} \\ \alpha \mathbf{S}_S^{ef} & -\alpha S_S^e \end{bmatrix}, \quad (21)$$

where ε_0 is the vacuum permittivity and $\alpha = 1/(1 - |k_x| \varepsilon_0 S_S^e)$. The effective surface permittivity ε_{eff} can be obtained using the G_{44} element of the Green's function as

$$\varepsilon_{eff}(k_x) = \frac{1}{|k_x| G_{44}} = \varepsilon_0 - \frac{1}{|k_x| S_S^e}, \quad (22)$$

As an example, the asymptotic method has been compared to the "exact" method in the calculation of the surface wave velocity. The free surface acoustic wave velocity for a ZnO/diamond/silicon layered semi-space shown in Figure 6 has been calculated as poles of the exact and asymptotic surface Green's function (21). The thicknesses of ZnO and diamond layers are 1μm and 20 μm respectively. The semi-space Si substrate is represented by the PML layer

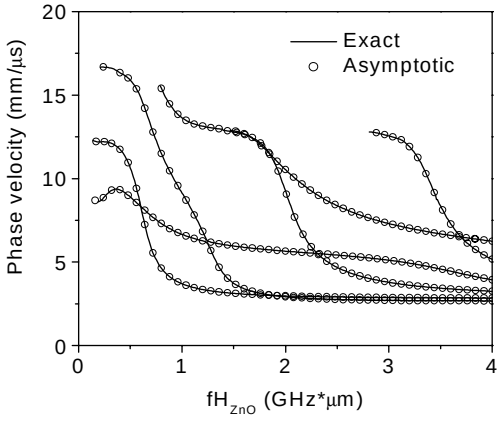

Figure 6: Surface wave velocity calculation for the ZnO/diamond/silicon layered semi-space using exact (solid lines) and asymptotic (open circles) surface stiffness matrix. Thickness of ZnO and diamond layers is 1 μm and 20 μm respectively. In exact computation, Si is a semispace. In the asymptotic calculation, the semispace Si substrate is represented by the PML layer.
with β=1.0+0.3i. The relative error of the asymptotic solution is around 10^{-10}.

Conclusions

Recent progress in modeling of ultrasonic wave propagation in layered arbitrarily anisotropic media has been reviewed. The efficient and stable recursive compliance/stiffness matrix method has been discussed. Using a simple second-order thin layer asymptotic expansion, the recursive stiffness matrix method has been further simplified and its computational efficiency has been improved. The asymptotic representation of the sublayers is an explicit function of the layer elastic constants and thickness; it maintains the energy balance of the propagating wave and system homogeneity, i. e., assures absence of scattering on the subdivided layer interfaces. For a semi-space substrate, a perfect matching layer (PML) method has been introduced and implemented. Both methods are computationally efficient and stable for arbitrarily layer thickness and frequency. Applications of these methods to surface acoustic wave analysis and ultrasonic characterization of multidirectional composite have been discussed.

References

[1] W. T. Thomson, "Transmission of elastic waves through a stratified solid medium," J. Appl. Phys., vol. 21, pp. 89-93, 1950.

[2] N. A. Haskell, "The dispersion of surface waves on stratified media," Bull. Seismol. Soc. Am., vol. 43, pp.17-34, 1953.

[3] L . M. Brekhovskikh, Waves in Layered Media Academic, New York, 1960.

[4] J. W. Dunkin, "Computations of modal solutions in layered elastic media at high frequencies," Bull. Seismol. Soc. Am., vol. 55, pp. 335-358, 1965.

[5] A. H. Fahmy and E. L. Adler, "Propagation of acoustic waves in multilayers: a matrix description," Appl. Phys. Lett. Vol. 20, pp. 495-497, 1973.

[6] S. I. Rokhlin, T. K. Bolland, and L. Adler, "Reflection and refraction of elastic waves on a plane interface between two generally anisotropic media," J. Acoust. Soc. Am., vol. 79, pp. 906-918, 1986.

[7] A. K. Mal, "Wave propagation in layered composite laminates under periodic surface loads," Wave Motion, vol. 9, pp. 231-238, 1988.

[8] F. B. Jensen, W. A. Kuperman, M. P. Porter, H. Schmidt, Computational Ocean Acoustics, Chap. 4., Springer, Berlin, 2000.

[9] E. L. Adler, "Matrix methods applied to acoustic waves in multilayers," IEEE Trans. Ultrason. Ferroelec. Freq. Contr., vol. 37, pp. 485-490, 1990.

[10] A. H. Nayfeh, "The general problem of elastic wave propagation in multilayered anisotropic media," J. Acoust. Soc. Am., vol. 89, pp.1521-1531, 1991.

[11] A. H. Nayfeh, Wave Propagation in Layered Anisotropic Media, North-Holland, Amsterdam, 1995.

[12] R. C. Y. Chin, G. W. Hedstrom and L. Thigpen, "Matrix methods in synthetic seismograms," Geophys. J. Astr. Soc., vol. 77, pp. 483-502, 1984.

[13] B. Hosten and M. Castaings, "Delta operator technique to improve the Thomson-Haskell-method stability for propagation in multilayered anisotropic absorbing plates," J. Acoust. Soc. Am., vol. 95, pp. 1931-1941, 1993.

[14] B. L. Kennett, Seismic Wave Propagation in Stratified Media. Cambridge University Press, New York, 1983.

[15] G. J. Fryer and L. N. Frazer, "Seismic waves in stratified anisotropic media", Geophys., J. R. Astron. Soc, vol. 78, pp. 691-710, 1984.

[16] S. I. Rokhlin and W. Huang, "Ultrasonic wave interaction with a thin anisotropic layer between two anisotropic solids: Exact and asymptotic-boundary-condition methods," J. Acoust. Soc. Am., vol. 92, pp. 1729-1742, 1992.

[17] B. Honein, A. M. B. Braga, P. Barbone, and G. Herrmann, "Wave propagation in piezoelectric layered media with some applications," J. Intelligent Mater. Syst. Struct., vol. 2, pp. 542-557, 1991.

[18] L. Wang and S. I. Rokhlin, "Stable reformulation of transfer matrix method for wave propagation in layered anisotropic media," Ultrasonics, vol. 39, pp. 407-418, 2001.

[19] L. Wang and S. I. Rokhlin, "Recursive stiffness matrix method for wave propagation in stratified media," Bull. Seism. Soc. Am., vol. 92, pp. 1129-1135, 2002.

[20] S. I. Rokhlin and L. Wang, "Stable recursive algorithm for elastic wave propagation in layered anisotropic media: stiffness matrix method," J. Acoust. Soc. Am., vol. 112, pp. 822-834, 2002.

[21] L. Wang and S. I. Rokhlin, "A compliance/stiffness matrix formulation of general Green's function and effective permittivity for piezoelectric multilayers," IEEE Trans. Ultrason. Ferroelec. Freq. Contr., submitted, 2003.

[22] L. Wang and S. I. Rokhlin "Recursive asymptotic stiffness matrix method for analysis of surface wave devices on layered piezoelectric media," Appl. Phys. Lett., vol. 81, pp. 4049-4052, 2002.

[23] L. Wang and S. I. Rokhlin, "Modeling of wave propagation in layered piezoelectric media by a recursive second-order asymptotic method," IEEE Trans. Ultrason. Ferroelec. Freq. Contr., submitted, 2003.

[24] D. E. Chimenti, "Guided waves in plates and their use in materials characterization," Appl. Mech. Rev., vol. 50, pp. 247-284, 1997.

[25] S. K. Datta, in "Comprehensive Composite Materials", Vol. 1, ed. T. W. Chou, Ch.1.18, Elsevier, pp. 511-558, 2000.

[26] L. Wang and S. I. Rokhlin, "Time resolved line focus acoustic microscopy of composites," IEEE Trans. Ultrason. Ferroelec. Freq. Contr., vol. 49, pp. 1231-1244, 2002.

[27] S. I. Rokhlin and L. Wang, "Ultrasonic waves in layered anisotropic media: characterization of multidirectional composites," Int. J. Solids and Struct. Vol. 39, pp. 4133-4149, 2002.

[28] S. I. Rokhlin and W. Huang, "Ultrasonic wave interaction with a thin anisotropic layer between two anisotropic solids: II. Second-order asymptotic boundary condition," J. Acoust. Soc. Am., vol. 94, pp. 3405-3420, 1993.

[29] D. Xiang, N. N. Hsu and G. V. Blessing, "The design, construction and application of a large aperture line-focus PVDF transducer", Ultrasonics, vol.34, pp.641-647, 1996.

Appendix: Fundamental acoustic tensor A

The fundamental acoustic tensor **A** for a piezoelectric medium is represented as [5, 21]

$$\mathbf{A}=\begin{bmatrix} k_x\mathbf{X}\boldsymbol{\Gamma}_{31} & -i\mathbf{X} \\ -i(\boldsymbol{\Gamma}_{11}-\boldsymbol{\Gamma}_{13}\mathbf{X}\boldsymbol{\Gamma}_{31})k_x^2+i\rho\omega^2\mathbf{I}' & k_x\boldsymbol{\Gamma}_{13}\mathbf{X} \end{bmatrix}, \quad \text{(A1)}$$

where ρ is the density of the solid and $\boldsymbol{\Gamma}_{ik}$ are the 4×4 matrices formed from the elastic constants c_{ijkl}, piezoelectric stress constants e_{ijk} and dielectric permittivity constants ε_{ik}:

$$\boldsymbol{\Gamma}_{ik}=\begin{bmatrix} c_{1i1k} & c_{1i2k} & c_{1i3k} & e_{k1i} \\ c_{2i1k} & c_{2i2k} & c_{2i3k} & e_{k2i} \\ c_{3i1k} & c_{3i2k} & c_{3i3k} & e_{k3i} \\ e_{i1k} & e_{i2k} & e_{i3k} & -\varepsilon_{ik} \end{bmatrix}. \quad \text{(A2)}$$

X is the inverse matrix of $\boldsymbol{\Gamma}_{33}$: $\mathbf{X}=\boldsymbol{\Gamma}_{33}^{-1}$. $\mathbf{I}'$ is the 4×4 identity matrix but with zero (4,4) element.